Article

Exploring the Effect of Glycerol and Hydrochloric Acid on Mesoporous Silica Synthesis: Application in Insulin Loading

May Kyaw Oo, Batoul Alallam, Abd Almonem Doolaanea, Alfi Khatib, Farahidah Mohamed,* and Bappaditya Chatterjee*

Read Online

| ACCESS | Metrics & More | Article Recommendations | Supporting Information |

ABSTRACT: Mesoporous silica (MPS), a carrier for active pharmaceutical ingredients, has a wide range of particle and pore morphology. A thorough understanding of ingredients used in MPS synthesis is an important prerequisite for optimizing its physicochemical characteristics. The present study aimed to evaluate the effect of glycerol and hydrochloric acid on the characteristics of synthesized MPS. Ordered MPS materials were synthesized using the pluronic P123 template and tetraethyl orthosilicate (TEOS) precursor. A three-level factorial design was employed to study the interaction between glycerol and hydrochloric acid. The optimized MPS particles were reasonably uniform in shape (short and rod-shaped) and < 1 μm in size with a smooth surface morphology. The nitrogen adsorption−desorption analysis revealed that the uniform cylindrical pores of the prepared MPS had a diameter > 5 nm and a total surface area > 500 m^2/g. With increasing acid and glycerol concentrations, the particle size of MPS decreased. However, while the glycerol increased the heterogeneity of the synthesized particles, the acid decreased it. The developed MPS was successfully loaded with a biological drug (insulin) with a 21.94% encapsulation efficiency. The MPS prepared in this study exhibits potential applications as a drug delivery carrier for drugs with a large molecular weight.

1. INTRODUCTION

Mesoporous silica (MPS) is a silica particle with uniform pores having diameters ranging from 2 to 50 nm.[1] MPS particles are commonly formed as rods and spheres, with pore structures varying according to the synthesis method, such as hexagonal, cubic, or lamellar arrays of pores.[2] MPS was first developed in 1990 by Yanagisawa, Shimizu, Kuroda, and Kato in Japan.[3] In recent years, MPS has gained the attention of formulation scientists due to its unique designable features.[4] As an advantage, MPS particles possess a high surface area where their particle size and pore size are tunable and customizable by adjusting the synthesis conditions or employing different surfactants in their synthesis preparation.[2,5]

It has demonstrated excellent properties of enhancing the bioavailability of poorly water-soluble drugs and improving drug loading due to it large surface area and ability to load the active pharmaceutical ingredients (API) within its nano-channels.[6] Many studies have shown that MPS as a drug carrier can improve the *in vitro* and *in vivo* dissolution of water-insoluble API by enhancing the trans-epithelial intestinal transport and thereby increasing the medication's oral bioavailability as a result.[7,8] Hence, customizing the particle size, pores, and surfaces of MPS has been carried out actively in pharmaceutical research to obtain the optimum MPS carrier for the API of interest during drug delivery.[2,5] MPS is reported

as being nontoxic, biocompatible, and thermally, hydro-thermally, and hydrolytically stable.[9]

Owing to the rapid technological advancements, various MPS types with a vast array of particle shapes and pore architectures have been produced and are widely used today.[6,10] Common varieties of MPS are Santa Barbara Amorphous type materials (SBA 15 and SBA 16), Mobil Composition of Matter (MCM 41 and MCM 48), Syloid materials, and Sylysia materials.[11,12]

MPS with ordered pores can be prepared using the Stober sol−gel process developed by Stober and Fink in 1968.[2] Tetraethyl orthosilicate (TEOS) is one of the most frequently used silica precursors. Other silica precursors, such as sodium silicate, amino silanes, and 3-mercaptopropyl trimethoxysilane, have also been utilized in MPS preparation.[14,15] The silica precursor forms polymer crosslinking in the surfactant template along with condensation events. In the presence of water, ethanol, and an acidic or basic catalyst [e.g., ammonia water, sodium hydroxide, and hydrochloric acid (HCl)], a
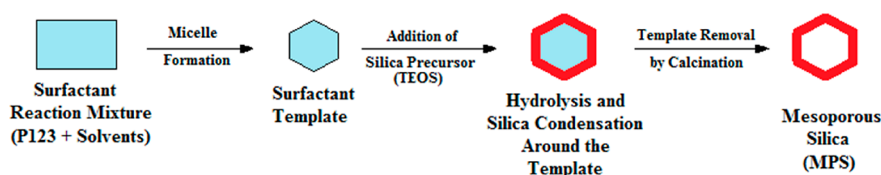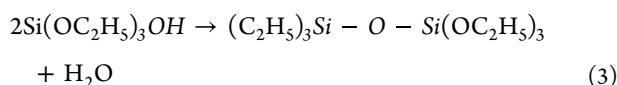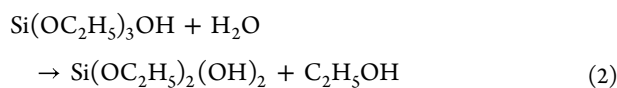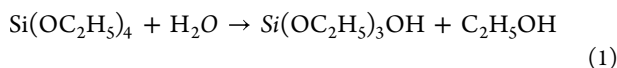
Figure 1. Basic flow chart of MPS synthesis.

silica network (Si−O−Si links) is constructed by converting TEOS to ethoxysilanols.[13] The hydrolysis reaction of TEOS silica precursor molecules and silica network formation can be simplified as mentioned in the following equations, eqs 1−3.[2]

$$Si(OC_2H_5)_4 + H_2O \rightarrow Si(OC_2H_5)_3OH + C_2H_5OH \tag{1}$$

$$Si(OC_2H_5)_3OH + H_2O$$
$$\rightarrow Si(OC_2H_5)_2(OH)_2 + C_2H_5OH \tag{2}$$

$$2Si(OC_2H_5)_3OH \rightarrow (C_2H_5)_3Si - O - Si(OC_2H_5)_3$$
$$+ H_2O \tag{3}$$

The general flow of MPS synthesis steps can be illustrated as shown in Figure 1. The MPS synthesis process starts with forming a template by the structure-directing agents: anionic, cationic, or a mixture of surfactants.[16] Surfactants such as cetyltrimethylammonium bromide (CTAB), dodecyl trimethylammonium bromide (DTAB), pluronic P123, sodium dodecyl sulfate, and glycerol are commonly employed.[5] The surfactant is dissolved in a selective solvent (e.g., water, ethanol, and glycerol−water mixture) to form self-arranging micelles as the backbone frame structure for the silica precursor.[2] In the last step, the surfactants can be removed from the MPS by calcination at a high temperature (> 500 °C) or by dissolving in an acidic solution at a specific pH to obtain the mesoporous structure.[7,17]

Apart from the silica precursor and surfactant template, the morphological characteristics of MPSs can also be influenced by many factors such as solvents, cosolvents, salts, catalysts, temperature, acidity, and stirring time. As a result of the synergetic influence of the components in the process, MPSs with a uniform particle size distribution can be developed.[7] Swelling agents such as ethyl acetate and 123 trimethyl benzene are typically utilized as co-templates to stabilize the silica condensation. Higher surfactant concentrations result in greater pore volume, whereas higher catalyst concentrations result in larger pore diameters, larger particle sizes, and lower pore volume.[15,17,18]

Glycerol, also known as 1,2,3-propanetriol, is a polar triol having three hydroxy groups. It has a molecular weight of 92.094 g/mol, a melting point of 20 °C, and a boiling point of 290 °C.[19] Glycerol is a viscous liquid with a dynamic viscosity of roughly 1300 mPa·s at 20 °C, making it significantly more viscous than water. It also has a higher density (1.25 ± 0.1 g/cm³) than water (0.9982 g/cm³). As a result, adding glycerol as a cosolvent would influence the formation of MPS particles since the density of the reaction medium will be higher.

HCl was commonly used during the MPS synthesis for providing an acidic reaction medium with low pH.[20,21] The concentration of HCl can affect the particle size, shape, and pore size of the MPS. In the synthesis where pluronic P123 was used as the template, the smaller short rod-shaped MPS

was derived at high HCl concentration.[22,23] Furthermore, HCl also plays a crucial role during the hydrothermal treatment in MPS synthesis, where the pore formation and expansion occur. Several reports have described the role of polar or nonpolar solvents and cosolvents during the MPS synthesis.[16,23−26] However, there are fewer reports describing the impact of their concentration on the MPS morphology. Hence, in this research, we aimed to study the effect of the glycerol amount and HCl concentration on MPS characteristics. This research has become unique as it sought to tune the size and polydispersity of MPS with a 3^2 factorial experimental design using Design of Expert (DOE) software, proceeding with insulin loading. Insulin is an antidiabetic polypeptide hormone that belongs to the biopharmaceutical classification system (BCS) class III. It is prescribed to type 1 and type 2 diabetic patients if their bodies can no longer produce insulin.[27] Hence, human insulin was used for loading in the optimized MPS in this research as it is still one of the most challenging biologics in the pharmaceutical research industry for oral delivery.[28,29]

2. RESULTS AND DISCUSSION

2.1. Optimization of MPS Synthesis Components. *2.1.1. Fitting the Variables and Optimization Model.* The relationship between the variables (concentrations of glycerol and HCl) and their responses were analyzed using a response surface model, a 3-level 2-factor factorial design. The design has generated nine randomized experiments comprising five replicates of center points. The independent variables were investigated, and the desired response variables are described in Table 1. Particle sizes varied from 739 to 1460 nm. The

**Table 1. Data of Variables for Optimization of MPS Synthesis with 3^2 Factorial Design**

Sample No.	Glycerol Amount (g)	HCl conc: (M)	Particle Size D_{50} (nm)	Polydispersity Index
			Dependent Variables	
1	0.9	1.5	1460	0.542
2	0.9	2	1190	0.389
3	0.9	2.5	1000	0.355
4	1.8	1.5	1180	0.555
5	1.8	2	863	0.554
6	1.8	2.5	807	0.513
7	2.7	1.5	1150	0.747
8	2.7	2	816	0.642
9	2.7	2.5	739	0.592

smallest particle size was measured at the composition with the highest glycerol content and the highest HCl concentration, whereas the lowest polydispersity index (PDI) (0.355 to 0.747) was observed with the lowest glycerol content and the highest HCl concentration.

For each level of factors, A and B, average values of R_1 and R_2 were calculated by comparing the reports on percent

Table 2. ANOVA Results of the RSM after Implementation of 3^2 Factorial Design

Responses	Experimental Design Model	p value	F value	R^2	Adjusted R^2	Predicted R^2	Adequate Precision
particle size D_{50} (R_1)	quadratic	< 0.0001	73.97	0.9898	0.9825	0.9053	38.713
polydispersity index (R_2)	linear	< 0.0001	56.59	0.9188	0.9026	0.8315	24.571
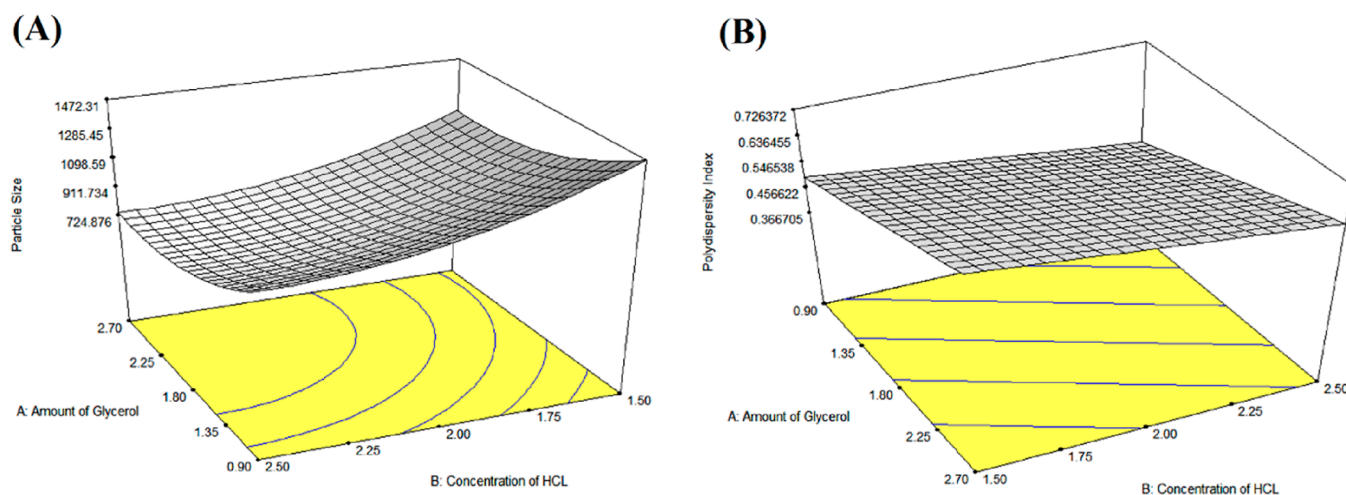
Figure 2. Three-dimensional RSM plot illustrating the effect of glycerol and HCl (A) on the particle size D_{50} of synthesized MPS particles and (B) on the PDI of the synthesized MPS particles.

increase or decrease, respectively. The particle size was decreased from an average of 1216 to 950 nm (21.92%) when the glycerol amount was increased from 0.9 to 1.8 g for different Hcl content. However, only a 5.09% size decrease could be achieved if the glycerol was increased further from 1.8 to 2.7 g. Similarly, increasing HCl concentration from 1.5 to 2 M caused a reduction in average particle size of synthesized MPS, from 1263 to 956 (24.30%). Still, when it was increased to 2.5 M, only an 11.26% size reduction was achieved. Hence, it can be concluded that the effect of these two variables on MPS particle size becomes less significant above a certain concentration level.

When the glycerol content was increased from 0.9 to 1.8 g, the PDI increased from 0.429 to 0.541 (26.13%). The same increment in the PDI (22.13%) was observed when the glycerol content was increased further to 2.7 g. In contrast, increasing the HCl concentration from 1.5 to 2 M resulted in the reduction of the PDI from 0.615 to 0.528 considering different glycerol content (14.05%). However, only a 7.89% PDI reduction was achieved when HCl concentration was increased to 2.5 M.

The fit summary of the model analysis (Table 2) showed that the experimental design models of both responses had an insignificant lack of fit with F values > 0.05. Hence, the models employed were considered adequate and well-fitting to proceed with the next step of the optimization process.

2.1.2. Effect of Independent Variables on MPS Particle Size. The influence of the independent variables on MPS particle size (R_1) was observed through the quadratic model since it had the best fit among all models with a probability > F value of less than 0.05. Summary of descriptive statistics obtained from analysis of variance (ANOVA) was used as a secondary check for the model's usefulness. Results are presented in Table 2.

Table 2 shows that the coefficient of determination values (R^2) of both responses were more than 0.9, which indicated that the data input was close enough to the fitted regression

line. The predicted R^2 value (0.9053) was reasonable with the adjusted R^2 value (0.9825). Subtraction of the predicted R^2 from the adjusted R^2 gave the difference of 0.0772 (cutoff < 0.2), indicating that the model fitted the input data and can reliably be used to interpolate.[30] Adequate precision was also checked to measure the signal-to-noise ratio. A ratio greater than 4 is considered desirable. Thus, the ratio of 38.713 indicated an excellent signal, and the model can be used to navigate the design space.[31]

$$R_1 = 869.38 - 157.50A - 207.33B + 12.25AB$$
$$+ 117.67A^2 + 108.17B^2 \qquad (4)$$

The quadratic equation (eq 4) and three-dimensional response surface methodology (RSM) plot (Figure 2A) derived using the DOE software represented the relationship between the independent variables and their responses. The significance of model terms was observed. The equation exhibited that both factors [glycerol amount (A) and HCl concentration (B)] affected the particle size of MPS during synthesis. The size of MPS can be significantly reduced ($p <$ 0.05) if a gradual or double increase in the glycerol amount or HCl concentration occurs individually (Table 3). However, the equation indicated that increasing both factors simultaneously will not have a significant effect as the p value of AB was 0.4065 ($p >$ 0.05).

2.1.3. Effect of Independent Variables on the PDI of MPS. The impact of two factors, glycerol amount (A) and HCl concentration (B), on the PDI (R_2) of the synthesized MPS particles was observed through the linear model. The linear model was the most suitable model compared to the other models, with a probability > F value of less than 0.05. The summary of ANOVA results is presented in Table 2.

Similar to R_1, the coefficient of determination (R^2) of R_2 was higher than 0.9, indicating the linearity of the data. The difference between the adjusted R^2 and predicted R^2 values was 0.0711 (cutoff < 0.2), which stated that the model was fit and

Table 3. Effect of Independent Variables (Factors) on the Dependent Variables (Responses) and Their Respective p Values

Factors	Particle Size D_{50} (R_1)		Polydispersity Index (R_2)	
	Effect	p value	Effect	p value
A	−157.50	< 0.0001	0.12	< 0.0001
B	−207.33	< 0.0001	−0.064	0.0004
AB	12.25	0.4065		
A^2	117.67	0.0002		
B^2	108.17	0.0003		

reliable to be used.[30] The adequate precision ratio was more than 4, indicating an excellent signal for the chosen experimental model.

$$R_2 = 0.55 + 0.12A - 0.064B \qquad (5)$$

The relationship between the independent variables and their responses was presented by the linear equation (eq 5) and three-dimensional RSM plot (Figure 2B) generated using the DOE software. From the R_2 model, it was observed that the glycerol amount (A) had a significant favorable influence ($p < 0.0001$) on the PDI of MPS particles, whereas HCl concentration (B) had a significant negative influence ($p = 0.0004$), indicating that the lower the glycerol content and the higher the HCL concentration during synthesis, the more uniform the MPS particles that could be produced. This could be because the higher acidity of the synthesis medium will cause a faster reaction, forming/creating smaller particles where the PDI result could appear uniform, but the particles might not have ordered shape or pores. The analysis results suggested that factors A and B had to be adjusted accordingly to optimize MPS synthesis for the desired responses.

2.1.4. Verification of the Optimized Solution Generated by RSM Analysis. Three possible compositions (checkpoints) and their predicted responses were chosen from the possible solutions generated using DOE software. These three checkpoints were prepared in triplicate and evaluated for two responses (R_1 and R_2), as described in Table 4. The percentage error between each of the predicted and corresponding actual responses was calculated to observe the closeness. All three checkpoint batches exhibited a low percentage error for R_1. However, a high percentage error (20.31%) was seen for the composition of 1.7 g of glycerol and 2 M HCl. Out of the three checkpoints, the composition with a glycerol amount of 1.5 g and a HCl concentration of 2 M showed the best closeness between predicted and actual responses with a lower percentage error. Hence, this composition was considered as an optimized solution and further characterized using Fourier transform infrared (FTIR) spectroscopy, scanning electron microscopy (SEM), transmission electron microscopy (TEM), and the Brunauer−Emmett−Teller (BET) method.

2.2. Characterization of the MPS Synthesized with the Optimized Glycerol−HCl Composition. *2.2.1. Functional Group Analysis.* Attenuated total reflection (ATR) spectra of starting materials of synthesis and MPS particles are presented in Figure 3. In addition, fumed silica was also tested and compared with synthesized MPS. In the glycerol spectrum, (O−H) stretching vibration showed a peak at 3292 waves/cm. The bands at 2934 and 2880 waves/cm represent (C−H) stretching, while the vibrations from the glycosidic linkage were seen as broad bands in the range of 850−994 waves/cm.[32,33]

The pluronic P123 spectrum (Figure 3A) exhibited a strong peak at 1099 waves/cm, representing the C−O−C stretching of the ether bond, a characteristic feature of the pluronic copolymer. IR peaks at 1242, 1372, and 2970 waves/cm were assigned to C−N stretching, CH_3 bending, and ═C−H bonds, respectively.[34,35] This bond, along with other distinctive peaks related to the PEO structure of pluronic P123, faded out after calcination. This result validated that P123 and glycerol, which were the template construction components, were successfully removed at the end of the synthesis to generate the pores of MPS.[36]

In the spectrum of TEOS, asymmetric and symmetric (CH_3) stretching were accountable for the bands found at 2974 and 2889 waves/cm, respectively, while the band located at 1167 could be due to (C−OH) stretching.[37−39] Bands at 1099, 961, and 475 waves/cm were due to asymmetric stretching vibration of (Si−O), (Si−O) pending vibration of non-condensed silanol groups, and (Si−O) bending vibration. The bands at 2974, 2889, and 1167 waves/cm faded after calcination, and only the bands at 1099, 961, and 475 waves/cm remained in the MPS spectrum, representing the characteristic features of MPS.

The spectrum of pure fumed silica was compared with the synthesized MPS spectrum in order to confirm the presence of a silica network in MPS particles. The weak band centered at 3667.5 waves/cm in the fumed silica spectra corresponded to the stretching vibration of the OH group, representing the hydrogen bonding between adsorbed water and the silica surface.[37,40] The small peak at 1632 waves/cm was due to OH group bending. The asymmetric stretching vibration of (Si−O) of the silica network produced a robust and broad band at approximately 1084 waves/cm. The peak at 809 waves/cm was due to symmetric stretching of Si−O−Si vibration, while the peak at 462.69 waves/cm was due to silica network (Si−O) bending vibration.

In the MPS spectrum (Figure 3B), the three functional regions at 1066, 959, and 446 corresponded to asymmetric stretching of the (Si−O) group, symmetric stretching of the (Si−O−Si) group, and (Si−O) bending vibrations, respectively.[32,37,41] These features represented the silica network, which again confirmed the successful synthesis of the MPS particles. The absence of characteristic absorption peaks

Table 4. Optimized Factors and Their Predicted and Experimental Responses with the Percentage Error

Solutions of Factors		Particle Size D_{50} in nm (R_1)		Polydispersity Index (R_2)		Percentage Error (%)	
Glycerol Amount (g)	HCl Conc: (M)	Predicted D_{50}	Mean Actual D_{50} ± SD ($n = 3$)	Predicted PDI	Mean Actual PDI ± SD ($n = 3$)	R_1	R_2
1	2.5	959	940 ± 156	0.419	0.462 ± 0.05	1.98	10.18
1.5	**2**	**964**	**941 ± 151**	**0.510**	**0.548 ± 0.05**	**2.39**	**7.5**
1.7	2	874	921 ± 65	0.522	0.628 ± 0.02	5.38	20.31
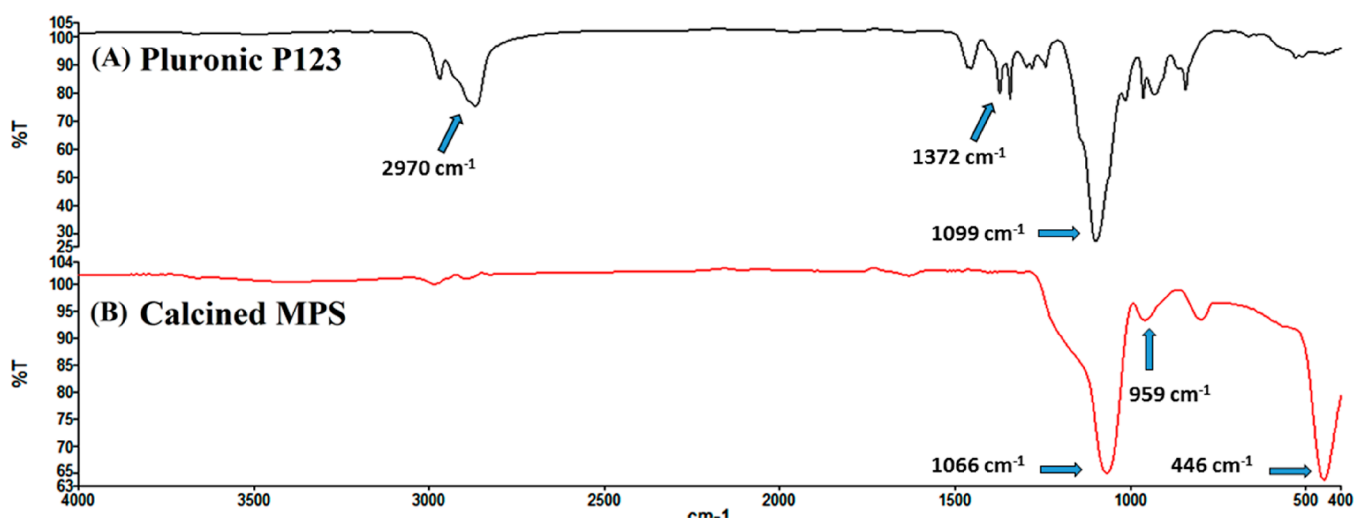
Figure 3. ATR spectra of (A) pure pluronic P123 polymer and (B) calcined MPS synthesized with the optimized composition.

related to surfactants clearly indicated that the template was successfully removed upon calcination.[42,43]

2.2.2. Scanning Electron Microscopy. The MPS particles before optimization (Figure 4A) were elongated and rod-
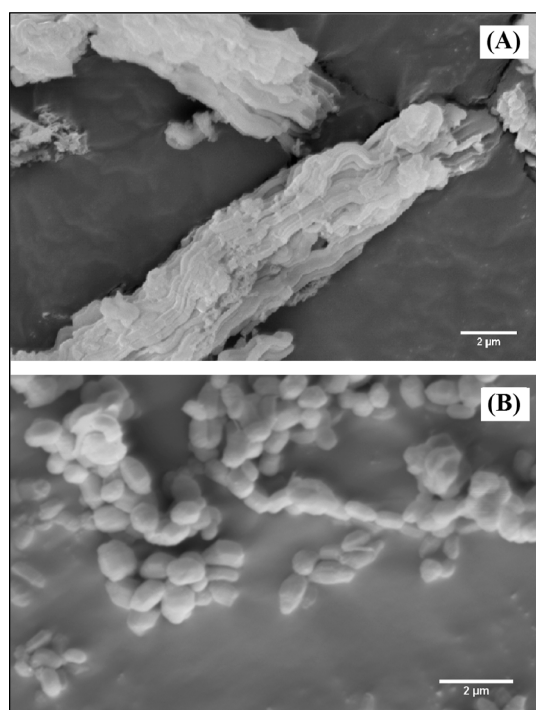

Figure 4. SEM image of MPS synthesized with (A) 1 M HCl without glycerol and (B) optimized glycerol−HCl composition.

shaped. The particles were highly aggregated and existed in chunks where some of the long rods were folded. Hence, precise size measurement of the individual particle was not possible. Their length seemed to be > 2 μm, and the width was < 400 nm. When the SEM image of improved MPS (Figure 4B) was evaluated using ImageJ version 1.49, the particles were found to be ordered, short, and rod-shaped with a length of 909 $\pm$ 134 nm and a width of 580 $\pm$ 112 nm with lesser aggregation. This result confirmed that the glycerol and HCl significantly affect the MPS particle shape and size during

synthesis. The surface of the particles appeared smooth, but the pores were not visible using SEM. Thus, TEM and BET analysis were carried out to confirm the presence of mesopores.

2.2.3. Transmission Electron Microscopy. The TEM image of optimized MPS (Figure 5) showed the MPS structure with a
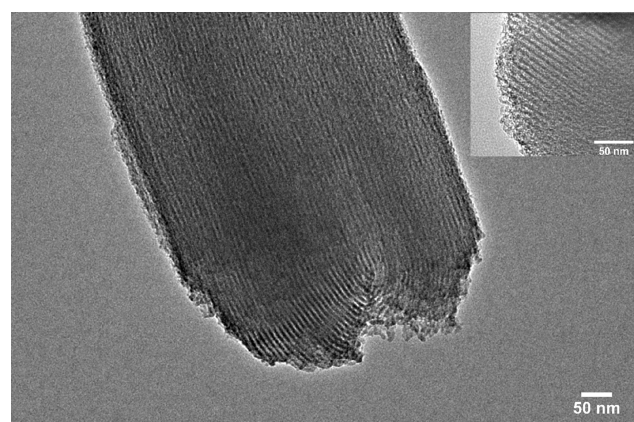
Figure 5. TEM image of the synthesized MPS with the optimized glycerol−HCl composition.

pore order. The estimated diameter of the pore was approximately 5 nm with a center-to-center pore distance of 9 nm. Elongated pores are visible in the TEM image. As the drug is to be loaded into the pores, the more the pores, the better the encapsulation. BET analysis was carried out later to provide more dimensional information about MPS pores.

2.2.4. Surface Area and Pore Volume Analysis. The presence of mesopores in the optimized MPS was confirmed from the adsorption−desorption diagram derived using the BET nitrogen adsorption technique. In the adsorption−desorption diagram of the optimized MPS derived using the BET nitrogen adsorption technique, the presence of mesopores was noticed (Figure 6A,B). In Figure 6A, a type IV isotherm was observed due to multilayer adsorption followed by capillary condensation in mesopores.[44] The vertical H1 hysteresis loop can be interpreted as the pores being in an array order and having a cylindrical shape with a highly uniform size. This pore arrangement was comparable to
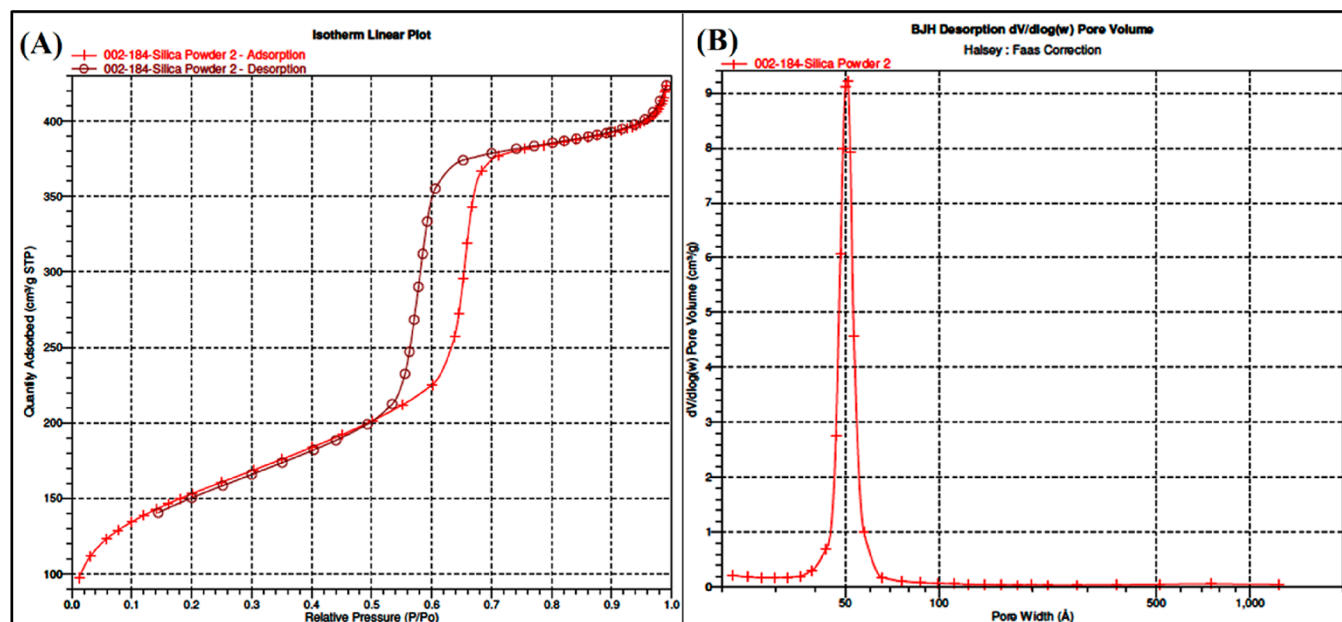
Figure 6. (A) Nitrogen adsorption/desorption isotherms and (B) BJH pore volume and pore size distribution of the synthesized MPS with the optimized glycerol−HCl composition.

that of the SBA 15 MPS type. The results showed a surface area of 543.9 ± 3.21 m^2/g, a BJH cumulative pore volume of 0.66 ± 0.04 cm^3/g, and an average pore width of 53.57 ± 25.80 (5.36 ± 2.58 nm).

2.3. Insulin Loading in MPS (Encapsulation Efficiency). The insulin was loaded in the pores of the optimized MPS. The high-performance liquid chromatography (HPLC) method, used to study the encapsulation efficiency, showed a good linearity ($R^2 = 0.9997$) within a concentration range of 2 to 120 μg/mL. The retention times of insulin peaks were 4.9 ± 0.2 min. The encapsulation efficiency of insulin was determined to be $21.94 \pm 0.24\%$. The amount of insulin loaded onto MPS (50 mg) was found to be 0.198 ± 0.021 mg. The derived encapsulation efficiency is relatively lower. Encapsulation efficiency depends on several factors, such as pore dimension, molecular weight of the actives, and method of encapsulation. We assume that the method of loading had a significant effect on encapsulation. We have used simple mixing of MPS and insulin for the minimum possible time to avoid environmental exposure. The mixing could be more intense using a mortar and pestle or stirring for longer time. Another possible reason could be shrinkage of pores during freeze-drying, forcing out insulin from the MPS. Therefore, further research is necessary to develop a better encapsulation method while keeping the dimension of the MPS same.

3. CONCLUSIONS

This study showed that glycerol and HCl reduced the particle size up to a certain degree, especially the length of the synthesized MPS. In the course of the present work, the desired particle size and uniformity of MPS were achieved after optimization the composition to 1.5 g of glycerol and 2 M HCl. With the increasing glycerol concentration, the MPS particle size decreased primarily in length. However, the increase in glycerol content could have caused more polydispersity in the MPS. The pH of the synthesis medium affected the particle size. The increase in molarity of HCl reduced the particle size and its uniformity. With the glycerol

and HCl, the resulted MPS particles were less agglomerated and more uniform in shape. The optimized MPS had short rod-shaped particles with cylindrical pore arrangements like the SBA-15 type. It also had a relatively high surface area and the required pore size. The developed MPS was able to load a high molecular weight drug (insulin) with 21.94% encapsulation efficiency. Although the drug loaded was only 0.198 mg or 5.7 IU, biologics such as insulin is very potent and its human equivalent dose needed is only 0.3 to 1 IU/kg of body weight.[45]

4. MATERIALS

Sigma-Aldrich (St. Louis, USA) supplied the poly(ethylene glycol)−poly(propylene glycol)−poly(ethylene glycol) polymer (pluronic P123), TEOS 98%, and glycerol 99.5%. Merck (Darmstadt, Germany) supplied potassium dihydrogen phosphate (KH_2PO_4), orthophosphoric acid (85%), HCl fuming (37%), absolute ethanol, acetonitrile (HPLC grade), and methanol (HPLC grade). Shaanxi Dideu Medichem Co. Ltd. (Shaanxi, China) provided lyophilized human insulin powder (99.2% with 23 IU/mg).

5. METHODS

5.1. MPS Synthesis. MPS particles were synthesized using the pluronic P123 polymer template and TEOS through the Stober sol−gel process in the presence of glycerol and an acidic environment. The surfactant template was prepared by constant stirring of 1.8 g of P123, glycerol (at various weights of 0.9, 1.8, and 2.7 g), and 69 mL of HCl (at varying concentrations of 1.5, 2, and 2.5 M) at 35 °C for 12 h till the solution turned clear. Then, 3.87 g of TEOS was added dropwise to the prepared solution under vigorous stirring. The stirring was continued for 5 min, followed by a static condition for 24 h at 35 °C and then aging at 100 °C for 24 h. The resultant solid particles were collected through centrifugation after repeated washing with distilled water. The product was dried at 80 °C for 24 h and calcined at 550 °C for 6 h in a furnace for template removal.

5.2. Optimization of MPS Synthesis. The optimized components of MPS were determined by a three-level factorial design (3^2) using the Design-Expert 6.0.10 (Stat-Ease Inc.)-mediated RSM. The variables (dependent and independent) and their levels are described in Table 5. The amount of

Table 5. Variables and Their Coded Level Values Used for Optimization[a]

Independent Variables (Factors)	Coded Levels			Dependent Variables (Responses)
	−1	0	1	
A: Glycerol Amount (g)	0.9	1.8	2.7	R_1: Particle Size D_{50} (nm)
B: HCl Concentration (M)	1.5	2	2.5	R_2: Polydispersity Index

[a]The amount of pluronic P123 was kept constant at 1.8 g against independent variables.

glycerol in grams (A) and concentration of HCl in Mole (B) were selected as independent variables as they can significantly affect the shape, size, and uniformity of MPS particles. The levels of the factors were determined based on the preliminary studies before the optimization. As the size and uniformity of carrier particles significantly influence the drug dissolution release and the bioavailability of drugs, the mean particle size at 50% diameter percentile aka D_{50} (R_1) and PDI (R_2) were taken as responses. The relationship between the factors and responses was studied and is reported.

The best fitted experimental model was chosen based on the lack of the fit test result (F values > 0.05) from the linear, two-factor interaction (2FI) and quadratic, cubic, and residual models. The significance of the model equation was also observed through ANOVA, multiple correlation coefficients (R^2), predicted R^2 values, and adjusted R^2 values. The optimization target criteria were set as < 1000 nm for the mean particle size D_{50} (R_1) and < 0.55 for the PDI (R_2). Small particles such as nanoparticles have the advantage of crossing barriers without causing embolic phenomena.[46] At the same time, larger particles will achieve higher drug loading and take longer durations to complete drug release and degrade. Generally, a smaller particle size is desired due to a higher surface area leading to higher solubility and enhanced bioavailability.[47] On the other hand, the larger particles can achieve higher drug loading and take longer durations to complete drug release and degrade. The lower the PDI, the higher the particle size uniformity. High PDI values near 1.0 indicate the polydisperse nature of the sample with multiple particle size populations.[48]

Three checkpoint batches were prepared following the predicted optimized compositions generated by the software, while the best-optimized composition formulation was chosen from the closeness of comparison. Percentage errors between the predicted and actual values of responses were calculated using eq 6.

$$\text{Percentage error} = [(R_{\text{Actual}} - R_{\text{Predicted}}) \div R_{\text{predicted}}] \times 100\% \qquad (6)$$

where R = responses of the model (particle size D_{50} and PDI).

5.3. Characterization of MPS. *5.3.1. Particle Size Distribution and Aggregation Analysis.* A Malvern nanosizer (Worcestershire, UK) was used to determine the particle size and PDI of the prepared MPS particles. At 25 °C, the MPS

particles (< 10 mg) were suspended in distilled water to check their sizes.

5.3.2. Functional Group Analysis. The functional groups of MPS particles, raw materials, and fumed silica powder were investigated utilizing the FTIR spectrometer (PerkinElmer, USA) using the ATR technique. The ATR diamond crystal scanned each sample powder (10 to 20 mg) for 15 scan accumulations at 2 waves/cm resolution within the IR radiation range of 4000−400 waves/cm at < 90 units force. The prominent peaks and bonds of resulting spectra were compared.

5.3.3. Particle and Pore Morphology Analysis. The size, shape, and surface morphology of the MPS particles were observed after gold coating using a ZEISS EVO 50 (Germany) scanning electron microscope. The particles were suspended in ethanol, placed onto a copper grid, and dried in a 50 °C oven for 30 min before being examined using a ZEISS Libra 120 (Germany) transmission electron microscope for their pore arrangement.

5.3.4. Surface Area and Pore Volume Analysis. Utilizing an Accelerated Surface Area and Porosimetry System 2020 Plus adsorption analyzer (Micromeritics, USA), nitrogen gas adsorption−desorption isotherms were investigated using the BET theory for surface area analysis, as well as Barrett−Joyner−Halenda (BJH) theory for pore size distribution. During the sample preparation step, in order to obtain exact specific surface area measurements, the samples (1 to 2 g) were vacuum-pumped and outgassed to remove the physically adsorbed gases and vapors. The samples were then dehydrated using nitrogen purging, and the volume of gas adsorbed to the surface of the particles was measured. At a relative pressure (P/P_0) of 0.97, the amount of adsorbed nitrogen gas and the total surface area of the particles, including pore volume, were correlated.

5.4. Insulin Loading of the Optimized MPS. The prepared optimized MPS was loaded with insulin through the physical sorption of API into the pores of the MPS using the solvent impregnation method.[49,50] Lyophilized human insulin (Insulin-P) was dissolved into a 100 μg/mL solution. Ten milliliters of this solution was added dropwise to 50 mg of the synthesized MPS carrier and mixed for 15 min. Then, the resultant insulin-loaded MPS particles (IMPS) were collected by centrifugation, gently washed three times with distilled water, and freeze-dried (Alpha 1-2 LD plus Christ, Germany) for 4 h.

5.4.1. Encapsulation Efficiency. During the collection process of drug-loaded MPS particles, the supernatant liquid was collected to determine the amount of free API that was not being loaded. Insulin-P solution (100 μg/mL) was considered as the amount of total API added. Both of the solutions were subjected to the reverse-phase HPLC method (Shimadzu LC-20AT, Japan) to determine the peak area of API. The mobile phase consisted of a 30:70 ACN:0.1 M KH_2PO_4 buffer with isocratic elution, with the pH corrected to 3.1 using orthophosphoric acid.[51] A C18 HPLC column (Agilent, California, USA) and a 0.8 mL/min flow rate were applied for insulin separation and detection at 214 nm wavelength. The encapsulation efficiency was calculated using the following equation, eq 7.[52,53]

Encapsulation efficiency

$$= \frac{\text{Amount of API added} - \text{free API}}{\text{Amount of API added}} \times 100\% \quad (7)$$

■ ASSOCIATED CONTENT

Ⓢ Supporting Information

The Supporting Information is available free of charge at https://pubs.acs.org/doi/10.1021/acsomega.2c01386.

Standard calibration graph of lyophilized human insulin (2−120 μg/mL), HPLC chromatogram of lyophilized human insulin (100 μg/mL), and HPLC chromatogram of free insulin (μg/mL) left in the filtrate after the drug loading onto MPS (50 mg) (PDF)

■ AUTHOR INFORMATION

Corresponding Authors

Farahidah Mohamed − *Pharmaceutical Technology Department, Kulliyah of Pharmacy, International Islamic University Malaysia, 25200 Kuantan, Pahang, Malaysia*; Phone: +91 224 233 2020; Email: bdpharmaju@gmail.com

Bappaditya Chatterjee − *Shobhaben Pratapbhai Patel School of Pharmacy and Technology Management, SVKM's NMIMS, 400056 Mumbai, India*; ⓞ orcid.org/0000-0003-1816-6028; Phone: +9 570 4000 (4843); Email: farahidah@iium.edu.my

Authors

May Kyaw Oo − *Pharmaceutical Technology Department, Kulliyah of Pharmacy, International Islamic University Malaysia, 25200 Kuantan, Pahang, Malaysia*

Batoul Alallam − *Advanced Medical and Dental Institute, Universiti Sains Malaysia, 13200 Kepala Batas, Penang, Malaysia*

Abd Almonem Doolaanea − *Pharmaceutical Technology Department, Kulliyah of Pharmacy, International Islamic University Malaysia, 25200 Kuantan, Pahang, Malaysia*

Alfi Khatib − *Department of Pharmaceutical Chemistry, Kulliyyah of Pharmacy, International Islamic University Malaysia, 25200 Kuantan, Malaysia*

Complete contact information is available at:
https://pubs.acs.org/10.1021/acsomega.2c01386

Author Contributions

The manuscript was written through the contributions of all authors. All authors have approved the final version of the manuscript.

Notes

The authors declare no competing financial interest.

■ ACKNOWLEDGMENTS

■ REFERENCES

(1) Thommes, M.; Kaneko, K.; Neimark, A. V.; Olivier, J. P.; Rodriguez-Reinoso, F.; Rouquerol, J.; Sing, K. S. W. Physisorption of Gases, with Special Reference to the Evaluation of Surface Area and Pore Size Distribution. *Pure Appl. Chem.* **2015**, *87*, 1051−1069.

(2) Schubert, U. Chemistry and Fundamentals of the Sol-Gel Process. In *The Sol−Gel Handbook*; David, L., Marcos, Z., Eds.; Wiley-VCH: Weinheim, 2015; pp 1−28.

(3) Yanagisawa, T.; Shimizu, T.; Kuroda, K.; Kato, C. The Preparation of Alkyltrimethylammonium-Kanemite Complexes and Their Conversion to Microporous Materials. *Bull. Chem. Soc. Jpn.* **1990**, *63*, 988−992.

(4) Chaudhari, S.; Gupte, A. Mesoporous Silica as a Carrier for Amorphous Solid Dispersion. *Br. J. Pharm. Res.* **2017**, *16*, 1−19.

(5) ALOthman, Z. A. Fundamental Aspects of Silicate Mesoporous Materials. *Materials* **2012**, *5*, 2874−2902.

(6) Menasco, D.; Wang, Q. Nanoparticles as Drug Delivery Vehicles. In *Drug delivery: Principles and Applications*; Wang, B., Hu, L., Siahaan, T. J., Eds.; John Wiley and Sons. Inc.: Hoboken, NJ, 2016; pp 299−335.

(7) Lodha, A.; Lodha, M.; Patel, A.; Chaudhuri, J.; Dalal, J.; Edwards, M.; Douroumis, D. Synthesis of Mesoporous Silica Nanoparticles and Drug Loading of Poorly Water Soluble Drug Cyclosporin A. *J. Pharm. BioAllied Sci.* **2012**, *4*, 92.

(8) Mellaerts, R.; Houthoofd, K.; Elen, K.; Chen, H.; Van Speybroeck, M.; Van Humbeeck, J.; Augustijns, P.; Mullens, J.; Van den Mooter, G.; Martens, J. A. Aging Behavior of Pharmaceutical Formulations of Itraconazole on SBA-15 Ordered Mesoporous Silica Carrier Material. *Microporous Mesoporous Mater.* **2010**, *130*, 154−161.

(9) US FDA. *Silicon Dioxide*.

(10) Biswas, N. Modified Mesoporous Silica Nanoparticles for Enhancing Oral Bioavailability and Antihypertensive Activity of Poorly Water Soluble Valsartan. *Eur. J. Pharm. Sci.* **2017**, *99*, 152−160.

(11) Qian, K. K.; Bogner, R. H. Application of Mesoporous Silicon Dioxide and Silicate in Oral Amorphous Drug Delivery Systems. *J. Pharm. Sci.* **2012**, *101*, 444−463.

(12) Wang, Y.; Sun, L.; Jiang, T.; Zhang, J.; Zhang, C.; Sun, C.; Deng, Y.; Sun, J.; Wang, S. The Investigation of MCM-48-Type and MCM-41-Type Mesoporous Silica as Oral Solid Dispersion Carriers for Water Insoluble Cilostazol. *Drug Dev. Ind. Pharm.* **2014**, *40*, 819−828.

(13) Stöber, W.; Fink, A.; Bohn, E. Controlled Growth of Monodispersed Silica Spheres in the Micron Size Range. *J. Colloid Interface Sci.* **1968**, *26*, 62−69.

(14) Rahmat, N.; Hamzah, F.; Sahiron, N.; Mazlan, M.; Zahari, M. M. Sodium Silicate as Source of Silica for Synthesis of Mesoporous SBA-15. *Mater. Sci. Eng.* **2016**, *133*, 1−9.

(15) Soto, R. J.; Yang, L.; Schoenfisch, M. H. Functionalized Mesoporous Silica via an Aminosilane Surfactant Ion Exchange Reaction: Controlled Scaffold Design and Nitric Oxide Release. *ACS Appl. Mater. Interfaces* **2016**, *8*, 2220−2231.

(16) Cao, L.; Shao, J. G.; Yang, Y. B.; Yang, Y. X.; Liu, X. N. Synthesis of Mesoporous Silica with Cationic-Anionic Surfactants. *Glass Phys. Chem.* **2010**, *36*, 182−189.

(17) Seo, J. W.; Lee, W.; Nam, S.; Ryoo, H. Mesoporous Structure Control of Silica in Room- Temperature Synthesis under Basic Conditions. *J. Nanomater.* **2014**, *2015*, 2−6.

(18) Wu, L.; Jiao, Z.; Wu, M.; Song, T.; Zhang, H. Formation of Mesoporous Silica Nanoparticles with Tunable Pore Structure as Promising Nanoreactor and Drug Delivery Vehicle. *Royal Soc. Chem. Adv.* **2016**, *6*, 13303−13311.

(19) PubChem. *Glycerol*.

(20) Fowler, C. E.; Khushalani, D.; Lebeau, B.; Mann, S. Nanoscale Materials with Mesostructured Interiors. *Adv. Mater.* **2001**, *13*, 649−652.

(21) Vatanparast, H.; Shahabi, F.; Bahramian, A.; Javadi, A.; Miller, R. The Role of Electrostatic Repulsion on Increasing Surface Activity of Anionic Surfactants in the Presence of Hydrophilic Silica Nanoparticles. *Sci. Rep.* **2018**, *8*, 7251.

(22) Ding, Y.; Yin, G.; Liao, X.; Huang, Z.; Chen, X.; Yao, Y.; Li, J. A Convenient Route to Synthesize SBA-15 Rods with Tunable Pore Length for Lysozyme Adsorption. *Microporous Mesoporous Mater.* **2013**, *170*, 45−51.

(23) Björk, E. M.; Söderlind, F.; Odén, M. Tuning the Shape of Mesoporous Silica Particles by Alterations in Parameter Space: From Rods to Platelets. *Langmuir* **2013**, *29*, 13551−13561.

(24) Bouchoucha, M.; Côté, M. F.; C Gaudreault, R.; Fortin, M. A.; Kleitz, F. Size-Controlled Functionalized Mesoporous Silica Nanoparticles for Tunable Drug Release and Enhanced Anti-Tumoral Activity. *Chem. Mater.* **2016**, *28*, 4243−4258.

(25) Cai, Q.; Luo, Z. S.; Pang, W. Q.; Fan, Y. W.; Chen, X. H.; Cui, F. Z. Dilute Solution Routes to Various Controllable Morphologies of MCM-41 Silica with a Basic Medium. *Chem. Mater.* **2001**, *13*, 258−263.

(26) Wang, X.; Zhang, Y.; Luo, W.; Elzatahry, A. A.; Cheng, X.; Alghamdi, A.; Abdullah, A. M.; Deng, Y.; Zhao, D. Synthesis of Ordered Mesoporous Silica with Tunable Morphologies and Pore Sizes via a Nonpolar Solvent-Assisted Stober Method. *Chem. Mater.* **2016**, *28*, 2356−2362.

(27) Patil, N. H.; Devarajan, P. V. Colloidal Carriers for Noninvasive Delivery of Insulin. In *Colloid and Interface Science in Pharmaceutical Research and Development*; Ohshima, H., Makino, K., Eds.; Elsevier B.V.: Amsterdam, 2014; pp 411−442.

(28) Sharma, G.; Sharma, A. R.; Nam, J. S.; Doss, G. P. C.; Lee, S. S.; Chakraborty, C. Nanoparticle Based Insulin Delivery System: The next Generation Efficient Therapy for Type 1 Diabetes. *J. Nanobiotechnol.* **2015**, *13*, 74.

(29) Hirlekar, R. S.; Patil, E. J.; Bhairy, S. R. Oral Insulin Delivery : Novel Strategies. *Asian J. Pharm.* **2017**, *11*, S434−S443.

(30) Stat-Ease. *Interpretation of R-squared*.

(31) Stat-Ease. *Adequate Precision*.

(32) Bradley, M. *FTIR Basic Organic Functional Group Reference Chart*.

(33) Mohammed, C.; Alhassan, Y.; Yargamji, G. I.; Garba, S.; Bello, Z.; Ifeyinwa, A. I. Composition and Characterization of Crude Glycerol from Biodiesel Production Using Neem Seed Oil. *J. Basic Appl. Chem.* **2011**, *1*, 80−84.

(34) Thu, P. T. T.; Dieu, H. T.; Phi, H. N.; Viet, N. N. T.; Kim, S. J.; Vo, V. Synthesis, Characterization and Phenol Adsorption of Carbonyl-Functionalized Mesoporous Silicas. *J. Porous Mater.* **2012**, *19*, 295−300.

(35) Han, P.; Liu, T.; Ji, X.; Tang, S. Morphology-Controlled Synthesis of Mesoporous Silica with Co-Template of Surfactant P123 and Ionic Liquid [Dmim]Cl. *Chin. Chem. Lett.* **2018**, *29*, 1305−1309.

(36) He, Z.; Alexandridis, P. Micellization Thermodynamics of Pluronic P123 (EO20PO70EO20) Amphiphilic Block Copolymer in Aqueous Ethylammonium Nitrate (EAN) Solutions. *Polymers* **2017**, *10*, 32.

(37) Wale, A.; Nalawade, A.; Ponrathnam, S.; Rajan, C. R.; Badiger, M. One-Pot Synthesis of Bimodal (Macro-Meso, Micro-Mesoporous) Silica by PolyHIPE: Parameter Studies. *J. Porous Mater.* **2020**, *27*, 263−275.

(38) Dayana, I.; Sembiring, T.; Tetuko, A. P.; Sembiring, K.; Maulida, N.; Cahyarani, Z.; Setiadi, E. A.; Asri, N. S.; Ginting, M.; Sebayang, P. The Effect of Tetraethyl Orthosilicate (TEOS) Additions as Silica Precursors on the Magnetite Nano-Particles (Fe3O4) Properties for the Application of Ferro-Lubricant. *J. Mol. Liq.* **2019**, *294*, 111557.

(39) Dudás, Z.; Len, A.; Ianăşi, C.; Paladini, G. Structural Modifications Caused by the Increasing MTES Amount in Hybrid MTES/TEOS-Based Silica Xerogels. *Mater. Charact.* **2020**, *167*, 110519.

(40) Fu, Y.; Ma, X.; Yang, Q.; Zong, X. The Effect of Fumed Silica on the Interfacial Stability in the Polymer Gel Electrolyte. *Mater. Lett.* **2003**, *57*, 1759−1764.

(41) Guha, A.; Biswas, N.; Bhattacharjee, K.; Sahoo, N.; Kuotsu, K. PH Responsive Cylindrical MSN for Oral Delivery of Insulin-Design, Fabrication and Evaluation. *Drug Delivery* **2016**, *23*, 3552−3561.

(42) Ahmadi, E.; Dehghannejad, N.; Hashemikia, S.; Ghasemnejad, M.; Tabebordbar, H. Synthesis and Surface Modification of Mesoporous Silica Nanoparticles and Its Application as Carriers for Sustained Drug Delivery. *Drug Delivery* **2014**, *21*, 164−172.

(43) Jin, Z.; Wang, X.; Cui, X. Synthesis and Characterization of Ordered and Cubic Mesoporous Silica Crystals under a Moderately Acidic Condition. *J. Mater. Sci.* **2007**, *42*, 465−471.

(44) Sing, K. S. W.; Everett, D. H.; Haul, R. A. W.; Moscou, L.; Pierotti, R. A.; Rouquerol, J.; Siemieniewska, T. Reporting Physisorption Data for Gas/Solid Systems with Special Reference to the Determination of Surface Area and Porosity. *Pure Appl. Chem.* **1985**, *57*, 603−619.

(45) MIMS. Actrapid (Novo Nordisk).

(46) Kohane, D. S. Microparticles and Nanoparticles for Drug Delivery. *Biotechnol. Bioeng.* **2007**, *96*, 203−209.

(47) Patel, P.; Patel, M. Enhanced Oral Bioavailability of Nintedanib Esylate with Nanostructured Lipid Carriers by Lymphatic Targeting: In Vitro, Cell Line and in Vivo Evaluation. *Eur. J. Pharm. Sci.* **2021**, *159*, 105715.

(48) Danaei, M.; Dehghankhold, M.; Ataei, S.; Hasanzadeh Davarani, F.; Javanmard, R.; Dokhani, A.; Khorasani, S.; Mozafari, M. R. Impact of Particle Size and Polydispersity Index on the Clinical Applications of Lipidic Nanocarrier Systems. *Pharmaceutics* **2018**, *10*, 57.

(49) Ahern, R. J.; Hanrahan, J. P.; Tobin, J. M.; Ryan, K. B.; Crean, A. M. Comparison of Fenofibrate-Mesoporous Silica Drug-Loading Processes for Enhanced Drug Delivery. *Eur. J. Pharm. Sci.* **2013**, *50*, 400−409.

(50) Siavashani, A. Z.; Nazarpak, M. H.; Bakhsh, F. F.; Toliyat, T.; Solati-Hashjin, M. Preparation of Mesoporous Silica Nanoparticles for Insulin Drug Delivery. *Adv. Mater. Res.* **2014**, *829*, 251−257.

(51) Najjar, A.; Alawi, M.; Abuheshmeh, N.; Sallam, A. A Rapid, Isocratic HPLC Method for Determination of Insulin and Its Degradation Product. *Adv. Pharm.* **2014**, *2014*, 749823.

(52) Yuan, L.; Tang, Q.; Yang, D.; Zhang, J. Z.; Zhang, F.; Hu, J. Preparation of PH-Responsive Mesoporous Silica Nanoparticles and Their Application in Controlled Drug Delivery. *J. Phys. Chem. C* **2011**, *115*, 9926−9932.

(53) Chuang, E. Y.; Lin, K. J.; Su, F. Y.; Mi, F. L.; Maiti, B.; Chen, C. T.; Wey, S. P.; Yen, T. C.; Juang, J. H.; Sung, H. W. Noninvasive Imaging Oral Absorption of Insulin Delivered by Nanoparticles and Its Stimulated Glucose Utilization in Controlling Postprandial Hyperglycemia during OGTT in Diabetic Rats. *J. Controlled Release* **2013**, *172*, 513−522.